Inorg. Chem. **2007**, *46*, 7064–7074

Luminescent Platinum(II) Complexes Containing Isoquinolinyl Indazolate Ligands: Synthetic Reaction Pathway and Photophysical Properties

Sheng-Yuan Chang, Jakka Kavitha, Jui-Yi Hung, and Yun Chi*

Department of Chemistry, National Tsing Hua University, Hsinchu 300, Taiwan

Yi-Ming Cheng, Elise Y. Li, Pi-Tai Chou,* and Gene-Hsiang Lee

Department of Chemistry and Instrumentation Center, National Taiwan University, Taipei 106, Taiwan

Arthur J. Carty*

Steacie Institute for Molecular Sciences, National Research Council, Ontario K1A 0R6, Canada

Received May 7, 2007

New Pt(II) dichloride complexes [Pt(1-iqdzH)Cl_2] (**2a**) and [Pt(3-iqdzH)Cl_2] (**2b**), in which idqzH = 1- or 3-isoquinolinyl indazole, were prepared by treatment of the corresponding indazoles with K_2PtCl_4 in aqueous HCl solution. Despite their nonemissive nature, these complexes could react with excess indazole, sodium picolinate, and 3-trifluoromethyl-5-(2-pyridyl) pyrazole [(fppz)H] to afford the respective **a** and **b** series of luminescent complexes [Pt(1-iqdz)(L^X)] and [Pt(3-iqdz)(L^X)], where L^X = 1-iqdz (**1a**), 3-iqdz (**1b**), pic (**3a**, **3b**), and fppz (**4a**, **4b**). Single-crystal X-ray diffraction studies of **1b**, **2a**, and **3b** revealed a planar molecular geometry without notable intermolecular Pt···Pt contact in the solid crystal, a result of the steric repulsion imposed by the bulky indazole fragments. For coordination complexes **1**, **3**, and **4**, photoluminescence in degassed CH_2Cl_2 revealed high quantum efficiency and short radiative lifetimes in the range of several microseconds. As supported by the spectral feature, the associated radiation lifetimes, and a computational approach based on time-dependent density function theory (TD-DFT), the origin of the emission is attributed to a mixed ^{3}MLCT/$^3\pi\pi$ transition. The TD-DFT approach further confirmed that, except for the series **1** complexes, the HOMO of 3-iqdz complexes **3b** and **4b** is much less located at the central Pt(II) atom than the HOMO orbitals of the respective 1-iqdz complexes **3a** and **4a**, leading to a smaller degree of MLCT contribution. Consequently, there are a blue-shifted emission signal and an inferior emission quantum yield for the 3-iqdz derivatives. OLED devices with a multilayer configuration of ITO/NPB/CBP:**3a**/BCP/Alq_3/LiF/Al were fabricated using a CBP layer doped with various concentrations of **3a**, ranging from 6% to 100%, within the emitting layer. The best device performance was realized using a 6% doping concentration, for which the external quantum yield of 4.93%, luminous efficiency of 12.19 cd/A, and power efficiency of 6.12 lm W^{-1} were observed at 20 mA/cm^2, while a maximum luminescence as high as 20296 cd/m^2 was also realized at 16 V, showing good prospect for the fabrication of Pt(II) based OLEDs.

The third-row transition metal complexes have been extensively utilized for the fabrication of various types of phosphorescent organic light emitting diodes (OLEDs).[1] The imposed strong spin−orbit coupling, which is made possible by introduction of a heavy transition metal element into the skeleton of the complexes, effectively breaks down the spin conservation rule, facilitating a change in multiplicity and

* To whom correspondence should be addressed. E-mail: ychi@mx.nthu.edu.tw (Y.C.); chop@ntu.edu.tw (P.-T.C.); carty.arthur@ic.gc.ca (A.J.C.). Fax: +886 3 572 0864 (Y.C.); +886 2 2369 5208 (P.-T.C); +1 613 953 7592 (A.J.C.).

(1) (a) Holder, E.; Langeveld, B. M. W.; Schubert, U. S. *Adv. Mater* **2005**, *17*, 1109. (b) Yersin, H. *Top. Curr. Chem.* **2004**, *241*, 1. (c) Welter, S.; Brunner, K.; Hofstraat, J. W.; De Cola, L. *Nature* **2003**, *421*, 54. (d) Sun, Y.; Giebink, N. C.; Kanno, H.; Ma, B.; Thompson, M. E.; Forrest, S. R. *Nature* **2006**, *440*, 908. (e) Chou, P. T.; Chi, Y. *Eur. J. Inorg. Chem.* **2006**, 3319.

10.1021/ic700877n CCC: $37.00
Published on Web 07/26/2007

the subsequent radiative transition from the triplet state to the ground state.[2] As a result, research activities regarding OLEDs are gradually shifting from traditional fluorescent dyes to the heavy transition-metal-based phosphorescent emitters, particularly to those possessing good thermal and electrochemical stability and superior luminescent quantum efficiency upon excitation.[3]

As for the core metal ion, Pt(II) centered complexes are selected as the subject materials for generation of high efficiency phosphorescence; however, due to their planar molecular geometry, significant intermolecular interactions are frequently observed in both fluid and solid states,[4] resulting in difficulties in assessing their fundamental photophysical properties and strategy for potential applications. It is thus apparent that more active synthetic and theoretical endeavors should be put forth for understanding and improving their luminescence behaviors. As for the strategic design of ligands, recently, various homoleptic and heteroleptic cyclometalated, heavy transition-metal complexes possessing 2-aryl substituted pyridine ligands have been intensively studied.[5] The results indicate a good correlation among their basic metal−ligand bonding characteristics, the excited-state properties, and the accompanying molecular architectures. The strong ligand-field influence of the cyclometalated ligands, in combination with the effective metal-to-ligand back π-bonding, renders the anticipated high efficiency phosphorescence. As a result, various ligand designs have been applied to the Pt(II) metal complexes in attempts to tune their excited-state properties such as electron and charge transport character, emission energy gap, lifetime, and quantum yield, etc.[6] Moreover, such active pursuits have led to the successful fabrication of white-emitting OLEDs using Pt(II) phosphorescent dopant in a single emissive layer.[7]

In a relevant approach, in order to explore the possible applications in fabrication of OLEDs, we have prepared several Pt(II)-based complexes with generalized formulas of $[Pt(N^N)_2]$, in which N^N represents the N-donor ligands derived from 2-pyridyl azolate and its derivatives.[8] Three

Chart 1

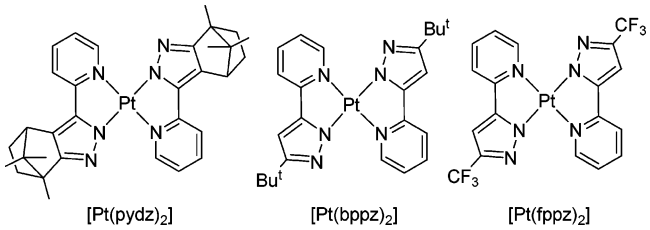

representative structural drawings are depicted in Chart 1, for which the accompanying studies have unraveled their molecular structure and stacking in the solid state, as well as the nature of the excited states that gave the highly efficient phosphorescence at room temperature. In this paper, we wish to present comprehensive studies on previously documented reactions involving a kind of pyridyl azole derivatives (denoted as N^NH) and K_2PtCl_4. Special attention is paid to several distinctive issues such as theoretical interpretation, possible synthetic pathways, and methods to broaden reactivity patterns using the newly isolated reaction intermediates. As for the practical approaches, one new complex [Pt(1-iqdz)(pic)] (**3a**) is demonstrated to show its capabilities in exhibiting decent electroluminescent properties.

Experimental Section

General Procedures. All reactions were performed under nitrogen atmosphere. Solvents were distilled from appropriate drying agents prior to use. Commercially available reagents were used

(2) (a) Matsushita, T.; Asada, T.; Koseki, S. *J. Phys. Chem. A* **2006**, *110*, 13295. (b) Forster, L. S. *Coord. Chem. Rev.* **2006**, *250*, 2023. (c) Matsushita, T.; Asada, T.; Koseki, S. *J. Phys. Chem. C* **2007**, *111*, 6897.

(3) (a) Lowry, M. S.; Bernhard, S. *Chem. Eur. J.* **2006**, *12*, 7970. (b) Chou, P. T.; Chi, Y. *Chem. Eur. J.* **2007**, *13*, 380. (c) Evans, R. C.; Douglas, P.; Winscom, C. J. *Coord. Chem. Rev.* **2006**, *250*, 2093. (d) Chi, Y.; Chou, P.-T. *Chem. Soc. Rev.* **2007**, *36*, DOI: 10.1039/b608951h.

(4) (a) Lai, S. W.; Che, C. M. *Top. Curr. Chem.* **2004**, *241*, 27. (b) Wadas, T. J.; Wang, Q. M.; Kim, Y. J.; Flaschenreim, C.; Blanton, T. N.; Eisenberg, R. *J. Am. Chem. Soc.* **2004**, *126*, 16841. (c) Lu, W.; Chan, M. C. W.; Zhu, N.; Che, C. M.; Li, C.; Hui, Z. *J. Am. Chem. Soc.* **2004**, *126*, 7639. (d) Pomestchenko, I. E.; Castellano, F. N. *J. Phys. Chem. A* **2004**, *108*, 3485. (e) Ma, B.; Li, J.; Djurovich, P. I.; Yousufuddin, M.; Bau, R.; Thompson, M. E. *J. Am. Chem. Soc.* **2005**, *127*, 28. (f) Yam, V. W.-W.; Chan, K. H. Y.; Wong, K. M. C.; Chu, B. W. K. *Angew. Chem., Int. Ed.* **2006**, *45*, 6169. (g) Lu, W.; Roy, V. A. L.; Che, C. M. *Chem. Commun.* **2006**, 3972. (h) Kui, S. C. F.; Chui, S. S. Y.; Che, C. M.; Zhu, N. *J. Am. Chem. Soc.* **2006**, *128*, 8297. (i) Forniés, J.; Fuertes, S.; Martín, A.; Sicilia, V.; Lalinde, E.; Moreno, M. T. *Chem. Eur. J.* **2006**, *12*, 8253. (j) Field, J. S.; Haines, R. J.; Ledwaba, L. P.; McGuire, R., Jr.; Munro, O. Q.; Low, M. R.; McMillin, D. R. *Dalton Trans.* **2007**, 192. (k) Scaffidi-Domianello, Y. Y.; Nazarov, A. A.; Haukka, M.; Galanski, M.; Keppler, B. K.; Schneider, J.; Du, P.; Eisenberg, R.; Kukushkin, V. Y. *Inorg. Chem.* **2007**, *46*, 4469.

(5) (a) You, Y.; An, C. G.; Lee, D. S.; Kim, J. J.; Park, S. Y. *J. Mater. Chem.* **2006**, *16*, 4706. (b) Wong, W. Y.; Ho, C. L.; Gao, Z. Q.; Mi, B. X.; Chen, C. H.; Cheah, K. W.; Lin, Z. *Angew. Chem., Int. Ed.* **2006**, *45*, 7800. (c) Li, E. Y.; Cheng, Y. M.; Hsu, C. C.; Chou, P. T.; Lee, G. H.; Lin, I. H.; Chi, Y.; Liu, C. S. *Inorg. Chem.* **2006**, *45*, 8041. (d) Wilkinson, A. J.; Puschmann, H.; Howard, J. A. K.; Foster, C. E.; Williams, J. A. G. *Inorg. Chem.* **2006**, *45*, 8685. (e) Obara, S.; Itabashi, M.; Okuda, F.; Tamaki, S.; Tanabe, Y.; Ishii, Y.; Nozaki, K.; Haga, M. a. *Inorg. Chem.* **2006**, *45*, 8907. (f) Ionkin, A. S.; Marshall, W. J.; Roe, D. C.; Wang, Y. *Dalton Trans.* **2006**, 2468. (g) You, Y.; Kim, K. S.; Ahn, T. K.; Kim, D.; Park, S. Y. *J. Phys. Chem. C* **2007**, *111*, 4052. (h) Wu, L. L.; Yang, C. H.; Sun, I. W.; Chu, S. Y.; Kao, P. C.; Huang, H. H. *Organometallics* **2007**, *26*, 2017. (i) Takizawa, S. Y.; Sasaki, Y.; Akhtaruzzaman, M.; Echizen, H.; Nishida, J. i.; Iwata, T.; Tokito, S.; Yamashita, Y. *J. Mater. Chem.* **2007**, *17*, 841. (j) Marin, V.; Holder, E.; Hoogenboom, R.; Schubert, U. S. *Chem. Soc. Rev.* **2007**, *36*, 618. (k) Liu, T.; Xia, B. H.; Zhou, X.; Zhang, H. X.; Pan, Q. J.; Gao, J. S. *Organometallics* **2007**, *26*, 143. (l) Dedeian, K.; Shi, J.; Forsythe, E.; Morton, D. C.; Zavalij, P. Y. *Inorg. Chem.* **2007**, *46*, 1603. (m) Chen, L.; You, H.; Yang, C.; Ma, D.; Qin, J. *Chem. Commun.* **2007**, 1352. (n) Bettington, S.; Tavasli, M.; Bryce, M. R.; Beeby, A.; Al-Attar, H.; Monkman, A. P. *Chem. Eur. J.* **2007**, *13*, 1423. (o) Chang, C.-J.; Yang, C.-H.; Chen, K.; Chi, Y.; Shu, C.-F.; Ho, M.-L.; Yeh, Y.-S.; Pi-Tai, C. *Dalton Trans.* **2007**, 1881.

(6) (a) Brooks, J.; Babayan, Y.; Lamansky, S.; Djurovich, P. I.; Tsyba, I.; Bau, R.; Thompson, M. E. *Inorg. Chem.* **2002**, *41*, 3055. (b) Wong, W. Y.; He, Z.; So, S. K.; Tong, K. L.; Lin, Z. *Organometallics* **2005**, *24*, 4079. (c) He, Z.; Wong, W. Y.; Yu, X.; Kwok, H. S.; Lin, Z. *Inorg. Chem.* **2006**, *45*, 10922.

(7) (a) Che, C. M.; Chan, S. C.; Xiang, H. F.; Chan, M. C. W.; Liu, Y.; Wang, Y. *Chem. Commun.* **2004**, 1484. (b) Ma, B.; Djurovich, P. I.; Garon, S.; Alleyne, B.; Thompson, M. E. *Adv. Funct. Mater.* **2006**, *16*, 2438. (c) Williams, E. L.; Haavisto, K.; Li, J.; Jabbour, G. E. *Adv. Mater* **2007**, *19*, 197.

(8) (a) Kavitha, J.; Chang, S. Y.; Chi, Y.; Yu, J. K.; Hu, Y. H.; Chou, P. T.; Peng, S. M.; Lee, G. H.; Tao, Y. T.; Chien, C. H.; Carty, A. J. *Adv. Funct. Mater.* **2005**, *15*, 223. (b) Chang, S. Y.; Kavitha, J.; Li, S. W.; Hsu, C. S.; Chi, Y.; Yeh, Y. S.; Chou, P. T.; Lee, G. H.; Carty, A. J.; Tao, Y. T.; Chien, C. H. *Inorg. Chem.* **2006**, *45*, 137.

without further purification unless otherwise stated. All reactions were monitored by precoated TLC plates (0.20 mm with fluorescent indicator UV_{254}). Flash column chromatography was carried out using silica gel (~230−400 mesh). The indazole chelates, 1-iqdzH and 3-iqdzH, were prepared using Claisen condensation, in which (1*R*)-(+)-camphor was reacted with ethyl 1-isoquinolinecarboxylate (or ethyl 3-isoquinolinecarboxylate) in refluxing THF solution, followed by treatment of the diketone intermediates with excess of hydrazine monohydrate and two drops of conc HCl in refluxing ethanol.[9] Mass spectra were obtained on a JEOL SX-102A instrument operating in electron impact (EI) or fast atom bombardment (FAB) mode. ^{1}H and ^{13}C NMR spectra were recorded on a Mercury-400 or a Varian INOVA-500 instrument; chemical shifts are quoted with respect to the internal standard tetramethylsilane for ^{1}H and ^{13}C NMR data. Elemental analysis was carried out with a Heraeus CHN-O rapid elementary analyzer.

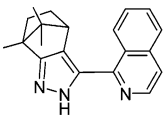

1-iqdzH

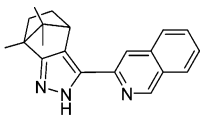

3-iqdzH

Spectroscopic and Dynamic Measurements. Steady-state absorption and emission spectra were recorded on a Hitachi (U-3310) spectrophotometer and an Edinburgh (FS920) fluorimeter, respectively. Both wavelength-dependent excitation and emission response of the fluorimeter were calibrated. A configuration of front-face excitation was used to measure the emission of the solid sample, in which the cell was made by assembling two edge-polished quartz plates with various Teflon spacers. A combination of appropriate filters was used to avoid interference from the scattering light. Lifetime studies were performed by an Edinburgh FL 900 photon-counting system with a hydrogen-filled or a nitrogen lamp as the excitation source. Data were analyzed using a nonlinear least-squares procedure in combination with an iterative convolution method. The emission decays were analyzed by the sum of exponential functions, which allows partial removal of the instrument time broadening and consequently renders a temporal resolution of ~200 ps.

To determine the photoluminescence quantum yield in solution, samples were degassed by three freeze−pump−thaw cycles under vigorous stirring conditions. 4-(Dicyanomethylene)-2-methyl-6-(*p*-dimethylaminostyryl)-4*H*-pyran (DCM, λ_{em} = 615 nm, Exciton, Inc.) in methanol was used as a reference, assuming a quantum yield of 0.43 with a 430 nm excitation.[10] An integrating sphere (Labsphere) was applied to measure the quantum yield in the solid state, in which the solid sample film was prepared via either spin coating or vapor deposition methods and was excited by argon ion laser line. The resulting luminescence was led to an intensified charge-coupled detector for subsequent quantum yield analyses. To obtain the PL quantum yield in solid state, the emission was collected via integrating sphere, and the quantum yield was calculated according to a reported method.[11]

Synthesis of [Pt(1-iqdz)$_2$] (1a). Method A. This compound was first prepared from a 1:2 mixture of K_2PtCl_4 and 1-iqdzH, for which the procedure has been described in our previous publication.[8a]

Method B. A solution of [Pt(1-iqdzH)Cl_2] (50 mg, 0.09 mmol) and 1-iqdzH (29 mg, 0.10 mmol) in 2-methoxyethanol was heated to 100 °C for 16 h. After that, the mixture was cooled to RT, and an excess of water was added. The precipitate was filtered, washed with diethyl ether, and dried under vacuum. The material was further purified by silica gel column chromatography (ethyl acetate and hexane = 1:1) and recrystallization from CH_2Cl_2 and hexane; yield: 44 mg and 62%.

Spectral data of **1a** follow: MS (FAB), *m*/*z* 800, M^+. ^{1}H NMR (400 MHz, CD_2Cl_2, 294 K): δ 10.93 (d, J = 6.4 Hz, 2H), 8.86 (d, J_{HH} = 8.2 Hz, 2H), 7.94 (d, J_{HH} = 7.8 Hz, 2H), 7.86 (dd, J_{HH} = 8.2, 7.0 Hz, 2H), 7.76 (dd, J_{HH} = 7.8, 7.0 Hz, 2H), 7.63 (d, J_{HH} = 6.4 Hz, 2H), 3.44 (d, J_{HH} = 2.8 Hz, 2H), 2.34 (m, 2H), 2.02 (m, 2H), ~1.58−1.47 (m, 4H), 1.52 (s, 6H), 1.09 (s, 6H), 0.85 (s, 6H). ^{13}C NMR (100 MHz, CD_2Cl_2, 294 K): δ 164.8 (2C), 156.5 (2C), 144.2 (2C), 142.1 (2C), 136.9 (2C), 132.1 (2C), 128.2 (2C), 127.8 (2C), 127.6 (2C), 126.9 (2C), 123.8 (2C), 118.4 (2C), 60.8 (2C), 52.8 (2C), 50.7 (2C), 34.1 (2C), 27.9 (2C), 20.5 (2C), 19.4 (2C), 10.9 (2C). Anal. Calcd for $C_{40}H_{40}N_6Pt$: C, 60.06; H, 5.04; N, 10.51. Found: C, 60.52; H, 5.29; N, 10.58.

Synthesis of [Pt(3-iqdz)$_2$] (1b). A solution of K_2PtCl_4 (100 mg, 0.24 mmol) and 3-iqdzH (160 mg, 0.53 mmol) in a mixture of 2-methoxyethanol (15 mL) and water (5 mL) was heated at 80 °C for about 16 h. After the solution was cooled to RT, the precipitate was filtered, washed with diethyl ether, and dried under vacuum to give yellow [Pt(3-iqdz)$_2$] (**1b**, 100 mg, 52%). Crystals of **1b** suitable for X-ray analysis were obtained by recrystallization from a mixture of dichloromethane and hexane at room temperature.

Spectra data of **1b** follow: MS (FAB), *m*/*z* 801, $(M + 1)^+$. ^{1}H NMR (400 MHz, $CDCl_3$, 294 K): δ 11.78 (s, 2H), 8.16 (d, J_{HH} = 8.1 Hz, 2H), ~7.81−7.73 (m, 6H), 7.55 (ddd, J_{HH} = 8.1, 6.7, 1.3 Hz, 2H), 3.17 (d, J_{HH} = 3.6 Hz, 2H), 2.20 (m, 2H), 1.92 (m, 2H), 1.50 (s, 6H), 1.46 (m, 2H), 1.29 (m, 2H), 1.03 (s, 6H), 0.85 (s, 6H). ^{13}C NMR (125 MHz, $CDCl_3$): δ 168.9 (2C), 157.3 (2C), 148.3 (2C), 142.2 (2C), 136.7 (2C), 132.9 (2C), 129.7 (2C),126.9 (2C) ,126.4 (2C), 126.1 (2C), 124.2 (2C), 113.4 (2C), 61.7 (2C), 50.7 (2C), 48.0 (2C), 34.0 (2C), 27.9 (2C), 20.9 (2C), 19.8 (2C), 11.2 (2C). Anal. Calcd for $C_{40}H_{40}N_6Pt$: C, 60.06; H, 5.04; N, 10.51. Found: C, 59.88; H, 5.23; N, 10.56.

Preparation of [Pt(1-iqdzH)Cl_2] and [Pt(3-iqdzH)Cl_2]. A solution of K_2PtCl_4 (200 mg, 0.48 mmol) and 1-iqdzH (146 mg, 0.48 mmol) in H_2O (15 mL) and 1 mL of HCl solution (4 M) was heated to reflux for about 2 h. After cooling the solution to RT, the precipitate was filtered, washed with diethyl ether, and dried under vacuum. This mixture was further purified by silica gel column chromatography (ethyl acetate and hexane = 2:1) and recrystallized from CH_2Cl_2 and hexane to give orange [Pt(1-iqdzH)-Cl_2] (**2a**, 171 mg, 63%) and red [Pt(1-iqdz)$_2$] (**1a**, 5 mg, 1%). The derivatives [Pt(3-iqdzH)Cl_2] (**2b**) and [Pt(3-iqdz)$_2$] (**1b**) were prepared in 69% and 1% yield using similar experimental procedures.

Spectral data of **2a** follow: MS (FAB, ^{195}Pt) *m*/*z* 569 $(M)^+$. ^{1}H NMR (400 MHz, $CDCl_3$, 298 K): δ 11.85 (s, 1H), 9.36 (d, J_{HH} = 6.8 Hz, 1H), 8.58 (d, J_{HH} = 8.4 Hz, 1H), 7.91 (d, J_{HH} = 3.6 Hz, 2H), 7.79 (m, 1H), 7.64 (d, J_{HH} = 6.8 Hz, 1H), 3.46 (d, J_{HH} = 3.6 Hz, 1H), 2.34 (m, 1H), 2.03 (ddd, J_{HH} = 12.3, 9.5, 2.9 Hz, 1H), 1.56 (td, J_{HH} = 10.7, 3.3 Hz, 1H), 1.47 (m, 1H), 1.43 (s, 3H), 1.05 (s, 3H), 0.84 (s, 3H). Anal. Calcd for $C_{20}H_{21}Cl_2N_3Pt$: C, 42.19; H, 3.72; N, 7.38. Found: C, 42.02; H, 4.03; N, 7.50.

(9) The synthetic methodology is somewhat related to those reported for the analogous (2-pyridyl) pyrazole ligands; see: (a) Wu, P. C.; Yu, J. K.; Song, Y. H.; Chi, Y.; Chou, P. T.; Peng, S. M.; Lee, G. H. *Organometallics* **2003**, *22*, 4938. (b) Cheng, C. C.; Yu, W. S.; Chou, P. T.; Peng, S. M.; Lee, G. H.; Wu, P. C.; Song, Y. H.; Chi, Y. *Chem. Commun.* **2003**, 2628.

(10) Drake, J. M.; Lesiecki, M. L.; Camaioni, D. M. *Chem. Phys. Lett.* **1985**, *113*, 530.

(11) de Mello, J. C.; Wittmann, H. F.; Friend, R. H. *Adv. Mater.* **1997**, *9*, 230.

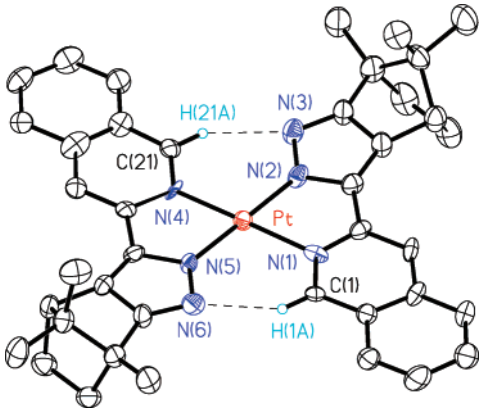

Figure 1. ORTEP diagram of **1b** with thermal ellipsoids shown at 50% probability level; selected bond lengths (Å) follow: Pt−N(1) = 2.105(6), Pt−N(2) = 2.000(7), Pt−N(4) = 1.998(4), and Pt−N(5) = 1.968(6).

Spectral data of **2b** follow: MS (FAB, ^{195}Pt) *m*/*z* 570 $(M + 1)^+$. ^{1}H NMR (400 MHz, $CDCl_3$, 298 K): δ 11.36 (br, 1H), 10.09 (s, 1H), 8.06 (d, J_{HH} = 8.0 Hz, 1H), 7.96 (s, 1H), 7.89 (d, J_{HH} = 9.6 Hz, 2H), 7.71 (m, 1H), 3.29 (d, J_{HH} = 3.6 Hz, 1H), 2.25 (m, 1H), 1.97 (ddd, J_{HH} = 12.7, 9.1, 3.7, 1H), 1.37 (s, 3H), 1.36 (m, 1H), 1.24 (m, 1H), 1.03 (s, 3H), 0.84 (s, 3H). Anal. Calcd for $C_{20}H_{21}Cl_2N_3Pt$: C, 42.19; H, 3.72; N, 7.38. Found: C, 42.20; H, 3.96; N, 7.52.

Synthesis of [Pt(1-iqdz)(pic)] and [Pt(3-iqdz)(pic)]. A solution of [Pt(1-iqdzH)Cl_2] (100 mg, 0.18 mmol), picolinic acid (54 mg, 0.44 mmol), and Na_2CO_3 (186 mg, 1.75 mmol) in 2-methoxyethanol (30 mL) was heated at 100 °C for 16 h. An excess of water was added after the solution was cooled to room temperature. The precipitate was filtered and dried under vacuum. Finally, this mixture was further purified by silica gel column chromatography (ethyl acetate and hexane = 1:1) and recrystallized from CH_2Cl_2 and hexane to give orange [Pt(1-iqdz)(pic)] (**3a**, 41 mg, 38%) and red [Pt(1-iqdz)$_2$] (**1a**, 8 mg, 6%). The derivatives [Pt(3-iqdz)(pic)] (**3b**) and [Pt(3-iqdz)$_2$] (**1b**) can be obtained in 44% and 4% yield under similar conditions. Single crystals of **3b** were obtained by recrystallization from a mixture of dichloromethane and hexane at room temperature.

Spectral data of **3a** follow: MS (FAB, ^{195}Pt) *m*/*z* 620 $(M + 1)^+$. ^{1}H NMR (400 MHz, $CDCl_3$, 298 K): δ 10.50 (d, J_{HH} = 6.2 Hz, 1H), 8.73 (m, 2H), 8.12 (dd, J_{HH} = 8.0, 7.4 Hz, 1H), 8.03 (d, J_{HH} = 7.6 Hz 1H), 7.85 (d, J_{HH} = 8.0 Hz, 1H), 7.79 (dd, J_{HH} = 7.6, 7.2 Hz, 1H), 7.71 (dd, J_{HH} = 7.4, 6.2 Hz, 2H), 7.44 (d, J_{HH} = 6.8 Hz, 1H), 3.34 (d, J_{HH} = 4.0 Hz, 1H), 2.25 (m, 1H), 1.92 (m, 1H), 1.43 (s, 3H), 1.39 (m, 2H), 1.02 (s, 3H), 0.81 (s, 3H). Anal. Calcd for $C_{26}H_{24}N_4O_2Pt$: C, 50.40; H, 3.90; N, 9.04. Found: C, 49.90; H, 4.09; N, 8.75.

Spectral data of **3b** follow: MS (FAB, ^{195}Pt) *m*/*z* 620 $(M + 1)^+$. ^{1}H NMR (400 MHz, $CDCl_3$, 298 K): δ 10.51 (d, J_{HH} = 5.6 Hz, 1H), 9.55 (s, 1H), 8.13 (dd, J_{HH} = 8.0, 7.4 Hz, 1H), 8.03 (m, 2H), 7.81 (m, 3H), 7.73 (dd, J_{HH} = 7.4, 5.6 Hz, 1H), 7.59 (dd, J_{HH} = 8.0, 7.2 Hz, 1H), 3.13 (d, J_{HH} = 3.2 Hz, 1H), 2.17 (m, 1H), 1.88 (m, 1H), 1.40 (s, 3H), 1.37 (m, 1H), 1.24 (m, 1H), 1.00 (s, 3H), 0.80 (s, 3H). Anal. Calcd for $C_{26}H_{24}N_4O_2Pt$: C, 50.40; H, 3.90; N, 9.04. Found: C, 49.95; H, 4.07; N, 8.96.

Synthesis of [Pt(1-iqdz)(fppz)] and [Pt(3-iqdz)(fppz)]. A solution of [Pt(1-iqdzH)Cl_2] (200 mg, 0.35 mmol) and (fppz)H (187 mg, 0.88 mmol) in ethanol was refluxed for 16 h. After this period, the reaction mixture was cooled and the solvent removed under vacuum. The residue was purified by silica gel column chromatography (ethyl acetate and hexane = 1:2), giving 6 mg of **1a** (2%), 4 mg of [Pt(fppz)$_2$] (2%), and 105 mg of [Pt(1-iqdz)(fppz)] (**4a**, 42%). Crystalline samples of **4a** were crystallized from ethyl acetate solution at room temperature. The 3-iqdz derivatives [Pt(3-iqdz)-(fppz)] (**4b**) and [Pt(3-iqdz)$_2$] (**1b**), together with the disubstituted complex [Pt(fppz)$_2$], were obtained in 39%, 3%, and 2% according to similar procedures.

Spectral data of **4a** follow: MS (FAB, ^{195}Pt) *m*/*z* 710 $(M + 1)^+$. ^{1}H NMR (400 MHz, d_6-acetone, 298 K): δ 11.04 (d, J_{HH} = 5.6 Hz, 1H), 10.46 (d, J_{HH} = 6.8 Hz, 1H), 8.85 (d, J_{HH} = 8.4 Hz, 1H), 8.21 (dd, J_{HH} = 7.6, 7.0 Hz, 1H), 8.06 (m, 2H), 7.95 (dd, J_{HH} = 8.9, 7.0 Hz, 1H), 7.87 (dd, J_{HH} = 8.9, 8.4 Hz, 1H), 7.76 (d, J_{HH} = 7.0 Hz, 1H), 7.53 (dd, J_{HH} = 7.6, 5.6 Hz, 1H), 7.20 (s, 1H), 3.49 (d, J_{HH} = 4.0 Hz, 1H), 2.33 (m, 1H), 1.99 (m, 1H) 1.42 (s, 3H), 1.39 (m, 2H), 1.06 (s, 3H), 0.82 (s, 3H). ^{19}F (470 MHz, d_6-acetone, 298 K): δ −61.12 (s, CF_3). Anal. Calcd for $C_{29}H_{25}F_3N_6$-Pt: C, 49.08; H, 3.55; N, 11.84. Found: C, 48.97; H, 3.75; N, 11.61.

Table 1. Crystal Data and Structure Refinement Parameters for Complexes **1b**, **2a**, and **3b**

	1b	**2a**	**3b**
empirical formula	$C_{40}H_{40}N_6Pt$	$C_{20}H_{21}Cl_2N_3Pt$	$C_{26}H_{24}N_4O_2Pt$
fw	799.87	569.39	619.58
T	295(2) K	150(1) K	150(1) K
cryst syst	orthorhombic	triclinic	monoclinic
space group	$P2_12_12_1$	$P\bar{1}$	$P2_1$
a	7.0868(3) Å	8.1514(1) Å	10.4558(1) Å
b	16.9811(8) Å	10.0314(2) Å	19.5010(2) Å
c	30.3358(15) Å	12.0138(2) Å	10.8625(1) Å
α		81.8893(9)°	
β		85.7748(11)°	96.9912(8)°
γ		83.3597(10)	
V, *Z*	3650.7(3) Å^3, 4	964.37(3) Å^3, 2	2198.38(4) Å^3, 4
density (calcd)	1.455 Mg/m^3	1.961 Mg/m^3	1.872 Mg/m^3
abs coeff	3.879 mm^{-1}	7.561 mm^{-1}	6.415 mm^{-1}
F(000)	1600	548	1208
cryst size (mm^3)	0.25 × 0.12 × 0.05	0.25 × 0.14 × 0.10	0.25 × 0.20 × 0.18
reflns collected	43030	15484	19249
indep reflns	8374 [*R*(int) = 0.0452]	4410 [*R*(int) = 0.0586]	8843 [*R*(int) = 0.0369]
max and min transmission	0.8297 and 0.4439	0.488 and 0.243	0.328 and 0.225
data/restraints/params	8374/0/424	4410/0/286	8843/1/602
GOF on F^2	1.295	1.100	1.038
final *R* indices [$I > 2\sigma(I)$]	R1 = 0.0553, wR2 = 0.1261	R1 = 0.0288, wR2 = 0.0647	R1 = 0.0262, wR2 = 0.0640
R indices (all data)	R1 = 0.0594, wR2 = 0.1280	R1 = 0.0356, wR2 = 0.0670	R1 = 0.0277, wR2 = 0.0647
largest diff peak and hole	1.580 and −2.574 e Å^{-3}	1.009 and −1.595 e Å^{-3}	1.925 and −1.479 e Å^{-3}

Spectral data of **4b** follow: MS (FAB, ^{195}Pt) *m*/*z* 710 $(M + 1)^+$. ^{1}H NMR (400 MHz, CD_2Cl_2, 298 K): δ 11.35 (s, 1H), 10.97 (dd, J_{HH} = 6.0, 1.1 Hz, 1H), 8.17 (d, J_{HH} = 8.1 Hz, 1H), 8.00 (td, J_{HH} = 7.5, 1.1 Hz, 1H), ~7.9−7.82 (m, 3H), 7.73 (dd, J_{HH} = 7.5, 1.3 Hz, 1H), 7.65 (ddd, J_{HH} = 8.1, 6.6, 1.6 Hz, 1H), 7.41 (ddd, J_{HH} = 7.5, 6.0, 1.3 Hz, 1H), 6.99 (s, 1H), 3.19 (d, J_{HH} = 4.0 Hz, 1H), 2.22 (m, 1H), 1.94 (m, 1H) 1.42 (s, 3H), 1.30 (m, 2H), 1.04 (s, 3H), 0.82 (s, 3H). ^{19}F (470 MHz, CD_2Cl_2, 298 K): δ −61.14 (s, CF_3). Anal. Calcd for $C_{29}H_{25}F_3N_6Pt$: C, 49.08; H, 3.55; N, 11.84. Found: C, 48.92; H, 3.67; N, 11.52

X-ray Structural Analysis. All single-crystal X-ray diffraction data were measured on a Bruker Smart CCD diffractometer using λ(Mo Kα) radiation (λ = 0.71073 Å). The data collection was executed using the SMART program. Cell refinement and data reduction were made with the SAINT program. The structure was determined using the SHELXTL/PC program and refined using full-matrix least-squares. All non-hydrogen atoms were refined anisotropically, whereas hydrogen atoms were placed at the calculated positions and included in the final stage of refinements with fixed parameters. The respective crystallographic refinement parameters are summarized in Table 1.

Computational Methodology. Time-dependent B3LYP calculations are based on the geometry optimized structures at B3LYP level. The basis set for the geometry optimization and the excitation energy calculation are both a double-ζ quality basis set consisting of Hay and Wadt's quasirelativistic effective core potentials (LANL2DZ) for Pt(II) atom;[12] a 6-31G* basis set was employed for the H, C, N, and O atoms. Typically, the lowest triplet and singlet roots of the nonhermitian eigenvalue equations were obtained to determine the vertical excitation energies. Oscillator strengths were deduced from the dipole transition matrix elements (for singlet states only). All the calculations were performed with the Gaussian 03 package.[13]

Results and Discussion

Synthesis and Characterization. The bidentate nitrogen chelates 1-iqdzH and 3-iqdzH were prepared from condensation of (1*R*)-(+)-camphor with ethyl 1-isoquinolinecarboxylate and with ethyl 3-isoquinolinecarboxylate, followed by treatment with excess of hydrazine monohydrate in refluxing ethanol. Treatment of 2 equiv of these chelates with K_2PtCl_4 in ethanol solution gave formation of the anticipated Pt(II) complexes **1a** and **1b** (Chart 2). It is noted that synthesis of 1-iqdz derivative **1a** was reported in our previous publication.[8a]

Chart 2

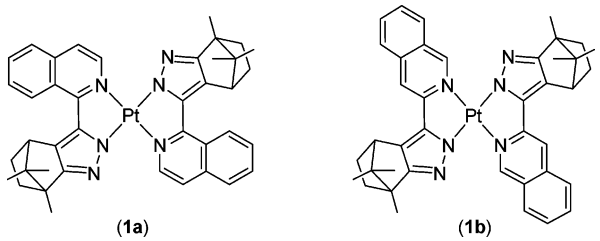

(**1a**) (**1b**)

Both Pt(II) complexes were characterized using routine spectroscopic methods as well as elemental analysis. Their spectroscopic data, particularly the unique ^{1}H NMR signals at δ 10.93 (**1a**) and 11.78 (**1b**), are in good agreement with the expected square planar, trans geometry, on which two indazole chelates were linked by a pair of interligand C−H···N interactions. Such a unique structural feature was confirmed by single-crystal X-ray analysis on **1b**. As shown in Figure 1, the nonbonding C−H···N interactions (C(1)−H(1A)···N(6) = 2.193 and C(21)−H(21A)···N(3) = 2.224 Å) between both ligands are comparable to those observed in the analogous, octahedral coordinated Ru(II) and Os(II) complexes.[14] The Pt···Pt span of ~9.185−9.257 Å versus that of 6.857 Å for **1a** showed minimal metal−metal contact in the solid state, which could be due the steric interference exerted by the indazolate fragments.[8a]

By adopting the synthetic protocols reported for the diimine complex $[Pt(bpy)Cl_2]$,[15] treatment of 1 equiv of these indazole ligands with K_2PtCl_4 in an aqueous HCl solution yielded neutral, chloride-substituted complexes $[Pt(1\text{-iqdzH})Cl_2]$ (**2a**) and $[Pt(3\text{-iqdzH})Cl_2]$ (**2b**) (Scheme 1). The presence of HCl is to provide a dual function for blocking the proton dissociation from the indazole chelates and for retardation of the chloride removal from the Pt(II) reagent K_2PtCl_4. These complexes impart high solubility in most common organic solvents such as acetone, THF, CH_2Cl_2, and $CHCl_3$, except water, alcohol, and aliphatic hydrocarbons. Their key spectral features are revealed by the observation of one sharp, downfield signal at δ 11.85 (**2a**) and 11.36 (**2b**) in the ^{1}H NMR spectra, which corresponds to the acidic N−H group of the coordinated indazole fragment. It was also notable that treatment of **2a** and **2b** with a stoichiometric amount of 1-iqdzH or 3-iqdzH gave formation of complexes **1a** and **1b** as expected. Such an observation unambiguously confirms the intermediacy of **2a** and **2b** en route to the initial formation of disubstituted complexes **1a** and **1b**, respectively.

To determine the salient structural features of complexes **2**, such as Pt−Cl and Pt−N bond distances as well as the molecular stacking in the solid state, single-crystal X-ray analysis on **2a** was undertaken, and an ORTEP drawing is

(12) (a) Hay, P. J.; Wadt, R. W. *J. Chem. Phys.* **1985**, *82*, 270. (b) Wadt, W. R.; Hay, P. J. *J. Chem. Phys.* **1985**, *82*, 284. (c) Hay, P. J.; Wadt, W. R. *J. Chem. Phys.* **1985**, *82*, 299.

(13) Frisch, M. J.; Trucks, G. W.; Schlegel, H. B.; Scuseria, G. E.; Robb, M. A.; Cheeseman, J. R.; Montgomery, J. A., Jr.,; Vreven, T.; Kudin, K. N.; Burant, J. C.; Millam, J. M.; Iyengar, S. S.; Tomasi, J.; Barone, V.; Mennucci, B.; Cossi, M.; Scalmani, G.; Rega, N.; Petersson, G. A.; Nakatsuji, H.; Hada, M.; Ehara, M.; Toyota, K.; Fukuda, R.; Hasegawa, J.; Ishida, M.; Nakajima, T.; Honda, Y.; Kitao, O.; Nakai, H.; Klene, M.; Li, X.; Knox, J. E.; Hratchian, H. P.; Cross, J. B.; Bakken, V.; Adamo, C.; Jaramillo, J.; Gomperts, R.; Stratmann, R. E.; Yazyev, O.; Austin, A. J.; Cammi, R.; Pomelli, C.; Ochterski, J. W.; Ayala, P. Y.; Morokuma, K.; Voth, G. A.; Salvador, P.; Dannenberg, J. J.; Zakrzewski, V. G.; Dapprich, S.; Daniels, A. D.; Strain, M. C.; Farkas, O.; Malick, D. K.; Rabuck, A. D.; Raghavachari, K.; Foresman, J. B.; Ortiz, J. V.; Cui, Q.; Baboul, A. G.; Clifford, S.; Cioslowski, J.; Stefanov, B. B.; Liu, G.; Liashenko, A.; Piskorz, P.; Komaromi, I.; Martin, R. L.; Fox, D. J.; Keith, T.; Al-Laham, M. A.; Peng, C. Y.; Nanayakkara, A.; Challacombe, M.; Gill, P. M. W.; Johnson, B.; Chen, W.; Wong, M. W.; Gonzalez, C.; Pople, J. A. *Gaussian 03*, revision C.02; Gaussian, Inc.: Wallingford, CT, 2004.

(14) (a) Tung, Y. L.; Wu, P. C.; Liu, C. S.; Chi, Y.; Yu, J. K.; Hu, Y. H.; Chou, P. T.; Peng, S. M.; Lee, G. H.; Tao, Y.; Carty, A. J.; Shu, C. F.; Wu, F. I. *Organometallics* **2004**, *23*, 3745. (b) Tung, Y. L.; Lee, S. W.; Chi, Y.; Chen, L. S.; Shu, C. F.; Wu, F. I.; Carty, A. J.; Chou, P. T.; Peng, S. M.; Lee, G. H. *Adv. Mater.* **2005**, *17*, 1059. (c) Tung, Y. L.; Chen, L. S.; Chi, Y.; Chou, P. T.; Cheng, Y. M.; Li, E. Y.; Lee, G. H.; Shu, C. F.; Wu, F. I.; Carty, A. J. *Adv. Funct. Mater.* **2006**, *16*, 1615.

(15) (a) Osborn, R. J.; Rogers, D. *J. Chem. Soc., Dalton Trans.* **1974**, 1002. (b) Egan, T. J.; Koch, K. R.; Swan, P. L.; Clarkson, C.; Van Schalkwyk, D. A.; Smith, P. J. *J. Med. Chem.* **2004**, *47*, 2926.

Scheme 1 [a]

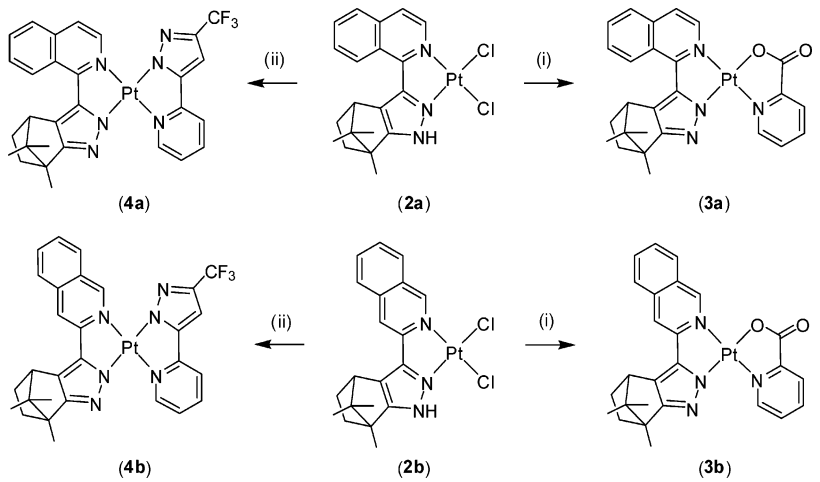

[a] (i) Picolinic acid, Na_2CO_3, 100 °C, 16 h; (ii) (fppz)H, 78 °C, 16 h.

shown in Figure 2. As expected, the Pt(II) metal element reveals a square-planar coordination geometry, and the shortest intermolecular Pt···Pt contact is calculated to be as long as 5.388 Å, indicating the presence of negligible intermolecular interaction. Although the Pt−N distance of the isoquinoline fragment (Pt−N(1) = 2.030(4) Å) is slightly longer than that of the indazole unit (Pt−N(2) = 1.979(4) Å), the averaged Pt−N bond distance is still comparable to that of **1b** as well as to those observed in the linear chain diimine analogue [(bpy)$PtCl_2$] (2.040 Å),[16] showing no significant alternation of Pt−N(indazolate) distance by retaining the proton at the uncoordinated nitrogen atom N(3). It is also notable that complex **2a** showed a parallel and tilted molecular stacking in the crystal lattice. The closest intermolecular Pt···Pt interaction is calculated to be 5.38 Å, which is again significantly longer than those (∼3.0−3.5 Å) reported for the columnar stacked Pt(II) complexes [(bpy)-$PtCl_2$] or [Pt(diimine)$_2$(CN)$_2$], diimine = bipyridine and biisoquinoline.[16]

Moreover, to expand the reaction scope, we also synthesized the corresponding heteroleptic metal complexes [Pt(1-iqdz)(pic)] (**3a**), [Pt(3-iqdz)(pic)] (**3b**), [Pt(1-iqdz)(fppz)] (**4a**), and [Pt(3-iqdz)(fppz)] (**4b**). These can be accomplished by conducting the ligand exchange reaction of **2a** and **2b** with picolinic acid or with 3-trifluoromethyl-5-(2-pyridyl)-pyrazole (fppz)H as the second chelating ligand in a way similar to that for other Pt(II) diimine complexes.[17] The success of these reactions reconfirms the nature of stepwise transfer for the proposed ligand assembly around the Pt(II) center. It is also noted that simultaneous isolation of a small amount of **1a**, **1b**, and [Pt(fppz)$_2$] was detected as coproducts, giving evidence for the possible occurrence of a much labile metal−ligand bonding in the intermediates **2a** and **2b**.

The single-crystal X-ray diffraction analysis on **3b** was conducted to unveil its stereoisomerism. As indicated in Figure 3, the neutral N-donor segments are located at the trans disposition, and the characteristic of slightly longer Pt−N distances (∼2.002−2.031 Å) is similar to those observed in two previous cases, namely **1b** and **2a**. For a comparison, the X-ray structural analyses of related cyclometalated Pt(II) complexes such as [Pt(ppy)$_2$] and [Pt(thppy)$_2$], thppy = 2-(2′-thienyl) pyridine, reveal that both pyridine fragments are oriented exclusively in a cis configuration despite the large distortion from the square planar geometry, i.e., a propeller type of ligand arrangement.[18] The result can be rationalized by the exceedingly strong trans effect exerted by the carbon atom of the phenyl or thiophene fragments, such that the pyridine fragments tend to reside at the cis orientation to avoid the competitive metal−ligand bonding. Conversely, the carboxylate and indazolate groups in **3b** display a much less directional effect, and their residence at the mutual trans dispositions is thermodynamically favorable. It is also worthy to note that for **3b** there exists a short N(4)···H(1A) contact of 2.337 Å between one ortho-H atom of picolinate and the noncoordinated N atom of the indazolate moiety. A consequence is given by the observation of an unusual downfield ^{1}H NMR chemical shift at δ 10.51.

Photophysical Measurements. The absorption and luminescence spectra recorded for **1**, **3**, and **4** in CH_2Cl_2 are depicted in Figures 4 and 5, while pertinent data are listed in Table 2. Several remarks can be pointed out from the corresponding spectroscopic and dynamic measurements. As shown in the absorption spectra, complexes **3** and **4** bearing iqdz chelates share spectral similarities in the lower lying electronic transitions. For example, the first transition band for **3a** (or **3b**) and **4a** (or **4b**) was located at ∼450 nm (434 nm) and 454 nm (427 nm), respectively. The results can be

(16) (a) Che, C. M.; He, L. Y.; Poon, C. K.; Mak, T. C. W. *Inorg. Chem.* **1989**, *28*, 3081. (b) Kato, M.; Sasano, K.; Kosuge, C.; Yamazaki, M.; Yano, S.; Kimura, M. *Inorg. Chem.* **1996**, *35*, 116. (c) Kato, M.; Kosuge, C.; Morii, K.; Ahn, J. S.; Kitagawa, H.; Mitani, T.; Matsushita, M.; Kato, T.; Yano, S.; Kimura, M. *Inorg. Chem.* **1999**, *38*, 1638. (d) Connick, W. B.; Henling, L. M.; Marsh, R. E.; Gray, H. B. *Inorg. Chem.* **1996**, *35*, 6261. (e) Connick, W. B.; Marsh, R. E.; Schaefer, W. P.; Gray, H. B. *Inorg. Chem.* **1997**, *36*, 913.

(17) (a) Hissler, M.; Connick, W. B.; Geiger, D. K.; McGarrah, J. E.; Lipa, D.; Lachicotte, R. J.; Eisenberg, R. *Inorg. Chem.* **2000**, *39*, 447. (b) Hissler, M.; McGarrah, J. E.; Connick, W. B.; Geiger, D. K.; Cummings, S. D.; Eisenberg, R. *Coord. Chem. Rev.* **2000**, *208*, 115.

(18) (a) Chassot, L.; Von Zelewsky, A. *Inorg. Chem.* **1987**, *26*, 2814. (b) Gianini, M.; Forster, A.; Haag, P.; von Zelewsky, A.; Stoeckli-Evans, H. *Inorg. Chem.* **1996**, *35*, 4889.

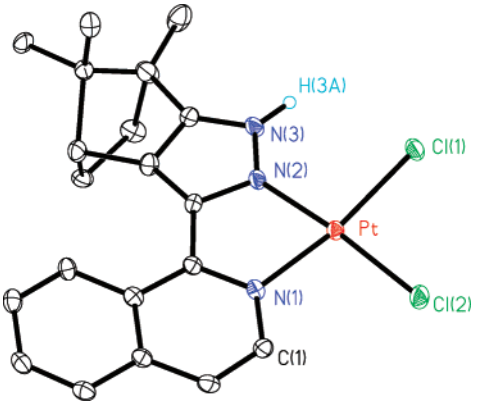

Figure 2. ORTEP diagram of **2a** with thermal ellipsoids shown at 50% probability level; selected bond lengths (Å) follow: Pt−N(1) = 2.030(4), Pt−N(2) = 1.979(4), Pt−Cl(1) = 2.292(1), and Pt−Cl(2) = 2.290(1).

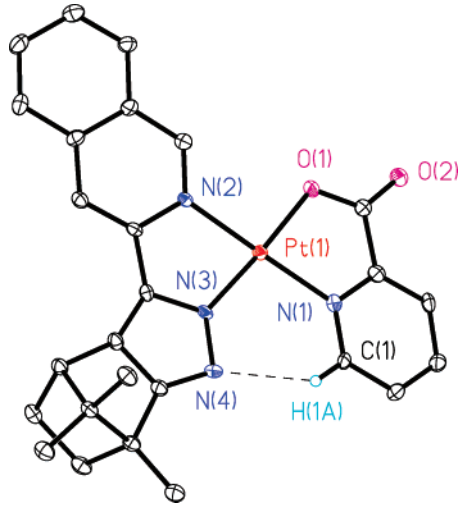

Figure 3. ORTEP diagram of **3b** with thermal ellipsoids shown at 50% probability level; selected bond lengths (Å) follow: Pt(1)−N(1) = 2.002-(4), Pt(1)−N(2) = 2.031(4), Pt(1)−N(3) = 1.978(4), and Pt(1)−O(1) = 2.028(4).

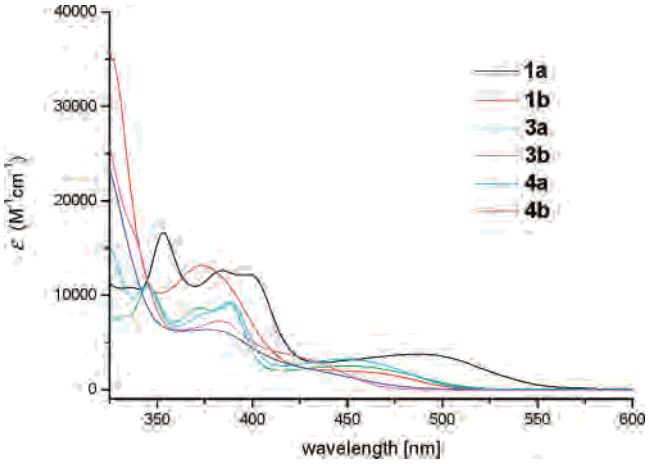

Figure 4. Absorption spectra of complexes **1a**−**4b** recorded in CH_2Cl_2 solution.

rationalized by the $S_0 \rightarrow S_1$ transition for **3a** (or **3b**) and **4a** (or **4b**) being mainly ascribed to the metal-to-ligand charge-transfer transition (MLCT) mixed with the intraligand charge-transfer transition (ILCT) from indazole to isoquinoline moieties, namely 1-iqdz for **3a** or **4a** and 3-iqdz for **3b** or

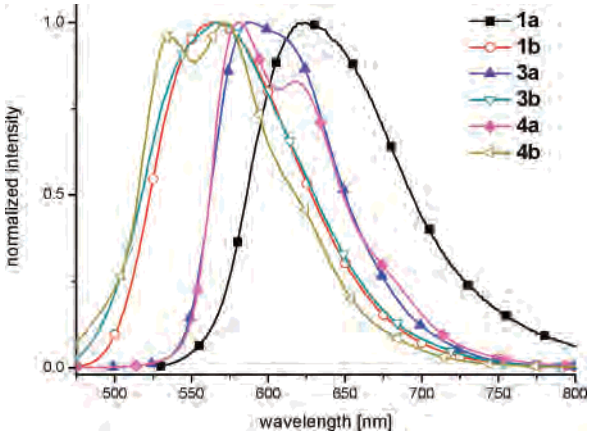

Figure 5. Normalized emission spectra of complexes **1a**−**4b** recorded in CH_2Cl_2 solution at RT.

4b, respectively. Further firm support of this viewpoint is rendered in the section describing the computational approaches.

Upon categorizing the titled compounds by **a** and **b** series that bear 1-iqdz and 3-iqdz ligands, respectively, the $S_0 \rightarrow S_1$ transition for series **a** derivatives tends to be red-shifted with respect to that of series **b** under the same iqdz ligands. For example, the $S_0 \rightarrow S_1$ peak wavelength for **1a**, **3a**, and **4a** of 502, 450, and 454 nm is a bathochromic shift by 40 nm (1730 cm^{-1}), 16 nm (820 cm^{-1}), and 27 nm (1400 cm^{-1}) compared to those of **1b** (462 nm), **3b** (434 nm), and **4b** (427 nm), respectively (see Table 2). The result can be tentatively rationalized by the more facile π-electron delocalization in the case of 1-iqdz (series **a**), lowering the π^* energy and hence a smaller energy gap of the mixed MLCT-($d_\pi \rightarrow \pi^*$)/ILCT($\pi \rightarrow \pi^*$) transition.[19] A similar distinction was observed for the 1-phenyl versus 3-phenyl isoquinoline ligands in the cyclometalated Ir(III) complexes, but an explicit answer has not yet been documented.[20] Further support of this viewpoint will be elucidated in the section describing theoretical approaches. In comparison to the pairs **3a**/**3b** and **4a**/**4b**, the anomalous red shift of 40 nm from **1a** to **1b** is intriguing. Note **3a** (or **3b**) and **4a** (or **4b**) are formed by replacing one of the iqdz ligands in **1a** (or **1b**) with less conjugated pic and fppz ligand, respectively. On the basis of the aforementioned facile π electron delocalization in 1-iqdz, the result can be rationalized by the existence of dual 1-iqdz ligands in **1a**, such that the π electrons can be further delocalized throughout the entire molecular framework, doubling its net delocalization efficiency with respect to **1b** bearing dual 3-iqdz ligands.

As for the emission shown in Figure 5, for all complexes studied, the origin of phosphorescence is unambiguous due to its significant O_2 quenching as well as the rather long

(19) (a) Hwang, F. M.; Chen, H. Y.; Chen, P. S.; Liu, C. S.; Chi, Y.; Shu, C. F.; Wu, F. I.; Chou, P. T.; Peng, S. M.; Lee, G. H. *Inorg. Chem.* **2005**, *44*, 1344. (b) Chang, C. J.; Yang, C. H.; Chen, K.; Chi, Y.; Shu, C. F.; Ho, M. L.; Yeh, Y. S.; Chou, P. T. *Dalton Trans.* **2007**, 1881.

(20) (a) Li, C. L.; Su, Y. J.; Tao, Y. T.; Chou, P. T.; Chien, C. H.; Cheng, C. C.; Liu, R. S. *Adv. Funct. Mater.* **2005**, *15*, 387. (b) Fang, K. H.; Wu, L. L.; Huang, Y. T.; Yang, C. H.; Sun, I.-W. *Inorg. Chim. Acta* **2006**, *359*, 441.

Table 2. Photophysical Properties of Pt(II) Complexes **1**−**4** in CH_2Cl_2 at Room Temperature

	UV−vis λ_{max}[a] ($\epsilon \times 10^3$, $M^{-1}\,cm^{-1}$)	em λ_{max} (nm)	Φ (%)	τ_{obs} (μs)	k_r	k_{nr}
1a	326 (11), 353 (17), 384 (13), 400 (12), 502 (3.5),	624	81	5.34	1.5×10^5	3.7×10^4
1b	327 (35), 374 (13), 462 (1.9)	567	24	1.65	1.4×10^5	4.7×10^5
3a	329 (7.7), 345 (11), 372 (8.7), 388 (9.2), 450 (2.5)	587 (612)[b] [621 nm][c]	64	8.2	7.8×10^4	4.4×10^4
3b	326 (23), 376 (6.4), 434 (2.0)	567	3.5	0.85	4.1×10^4	1.1×10^6
4a	326 (15), 344 (11), 372 (7.9), 389 (9.1), 454 (3.2)	581 (619)[b]	87	17	5.1×10^4	7.8×10^3
4b	326 (25), 383 (7.3), 427 (3.4)	535 (572)[b]	12	12.4	9.6×10^3	7.1×10^4

[a] The systematic error of the absorption coefficients measurement is ~±20%. [b] Shoulder. [c] As a vacuum deposited solid thin film. Note that in order to have a fair comparison, the absorption extinction coefficient of **1a**, which was reported in our previous report (ref 8a), has been reinvestigated to be 3500 ± 700 $M^{-1}\,cm^{-1}$ (at 502 nm).

emission lifetime of microseconds (see Table 2). In a good correlation with the trend of absorption spectra, the emission peak wavelength of series **a** complexes all revealed a red shift with respect to that of the **b** series bearing the same iqdz ligands (see Figure 5 and Table 2). More interestingly, in the room temperature, degassed CH_2Cl_2 solution, all of the series **a** complexes exhibit a more intense emission yield as compared to that of series **b** complexes. With emission quantum yield and observed lifetime provided, both radiative and nonradiative decay rates can be deduced, and the values are listed in Table 2. While the deduced radiative decay rates, k_r, for **1a** ($1.5 \times 10^5\ s^{-1}$) and **1b** ($1.4 \times 10^5\ s^{-1}$) are nearly identical, the main difference in emission yield lies in approximately 1 order of magnitude difference in the nonradiative decay rate k_{nr}, namely $3.7 \times 10^4\ s^{-1}$ and $4.7 \times 10^5\ s^{-1}$ for **1a** and **1b**, respectively. The results can be rationalized by further extended delocalization of the electron density in **1a**, such that the electronic excitation is equally spread among various degenerate states of the associated chromophores. The net result not only stabilizes the molecular framework but also reduces the radiationless deactivation processes plausibly due to the resulting steeper potential energy surfaces.[21] A similar viewpoint can be applied to the significant difference in radiationless transition between **3a** and **3b** (or **4a** and **4b**) bearing the same iqdz ligands. For example, k_{nr} for **3b** ($1.1 \times 10^6\ s^{-1}$, see Table 2) is larger than that of **3a** ($4.4 \times 10^4\ s^{-1}$) by 25-fold. An equally interesting remark is that the radiative decay rate for **3a** and **4a** is calculated to be larger than that for **3b** and **4b** by nearly 2- and 5-fold, respectively. In comparison to the series **b** complexes, the increase (decrease) of the radiative (nonradiative) decay rate leads to a significant increase of the emission quantum efficiency for series **a** complexes.

Theoretically, the larger radiative decay rate corresponds to a more allowed S_0-T_1 transition. On the basis of the first order approximation, it also implies the enhancement of spin−orbit coupling integral, most likely from the more d_π contribution of the core heavy metal atom Pt(II). In other words, in comparison with that of **3b** and **4b**, the experimental results render a proposal of greater MLCT contribution for **3a** and **4a** complexes in the T_1 manifold. Supplementary support of these viewpoints is given from the theoretical approach elaborated as follows.

(21) (a) Lo, S. C.; Shipley, C. P.; Bera, R. N.; Harding, R. E.; Cowley, A. R.; Burn, P. L.; Samuel, I. D. W. *Chem. Mater.* **2006**, *18*, 5119. (b) Yang, C. H.; Cheng, Y. M.; Chi, Y.; Hsu, C. J.; Fang, F. C.; Wang, K. T.; Chou, P. T.; Tsai, M. H.; Wu, C. C. *Angew. Chem., Int. Ed.* **2007**, *46*, 2418.

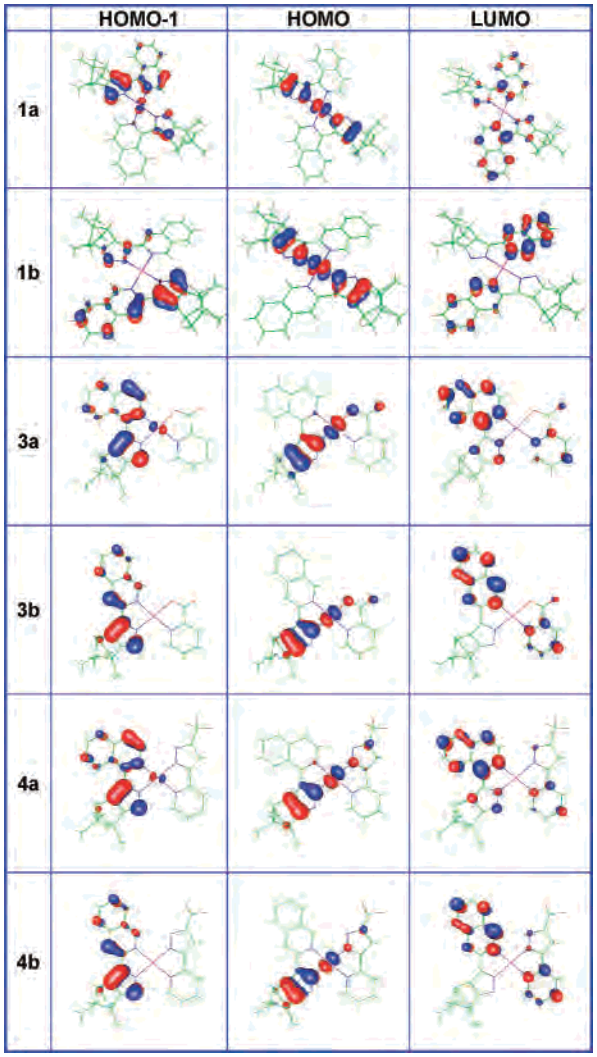

Figure 6. Representative frontier orbitals for complexes **1a**−**4b**.

Theoretical Approach. Theoretical confirmation of the underlying basis for the photophysical properties of the studied complexes was provided by the density functional theory (DFT) MO calculations. With the use of the TD-B3LYP method incorporating the B3LYP/LANL2DZ and 6-31G* optimized geometry, the vertical (i.e., Franck−Condon) excitation energy from the ground state to low-lying excited states was calculated. Figure 6 depicts the features of the lowest unoccupied molecular orbital (LUMO) and the two highest occupied (HOMO and HOMO − 1) frontier orbitals for complexes **1**, **3**, and **4**, which are mainly involved in the lower-lying transitions. The descriptions and the energy gaps of all complexes are listed

Table 3. Calculated Lowest Singlet and Triplet Excitations

	state	λ [nm]	f	assignment[a]	MLCT percentile (%)
1a	T_1	591.6	~0	HOMO → LUMO (76%)	17.1
				HOMO − 1 → LUMO (11%)	
				HOMO − 1 → LUMO + 1 (10%)	
	S_1	536.4	0.0741	HOMO → LUMO (94%)	20.8
1b	T_1	557.4	~0	HOMO → LUMO (73%)	16.1
				HOMO − 1 → LUMO + 1 (15%)	
	S_1	523.1	0.0042	HOMO → LUMO (98%)	21.9
3a	T_1	572.3	~0	HOMO → LUMO (+79%)	19.8
				HOMO − 1 → LUMO (21%)	
	S_1	489.9	0.0357	HOMO → LUMO (+94%)	23.0
3b	T_1	526.5	~0	HOMO − 1 → LUMO (+42%)	4.2
				HOMO − 1 → LUMO + 1 (+23%)	
				HOMO → LUMO (21%)	
	S_1	478.6	0.0083	HOMO → LUMO (+97%)	23.8
4a	T_1	561.8	~0	HOMO → LUMO (+55%)	11.6
				HOMO-1 → LUMO (46%)	
	S_1	476.5	0.0434	HOMO → LUMO (+95%)	19.8
4b	T_1	515.4	~0	HOMO − 1 → LUMO (+37%)	0.2
				HOMO − 1 → LUMO + 1 (+36%)	
	S_1	458.9	0.0203	HOMO → LUMO (+97%)	20.2

[a] The contributions of less than 10% were omitted for the qualitative discussion.

Table 4. Performance Characteristics for ITO/NPB/CBP:**3a**/BCP/Alq/LiF/Al

conc (%)	max lum[a] [cd m^{-2} (V)]	quantum eff[b] [%]	luminous eff[b] [cd A^{-1}]	power eff[b] [lm W^{-1}]	λ_{max}[c] (C.I.E.)
6%	20296 (16.0)	4.93 (3.16)	12.19 (7.82)	6.12 (2.96)	581, 612 (0.57, 0.43)
12%	12248 (16.0)	1.52 (1.30)	3.64 (3.11)	2.03 (1.27)	584, 614 (0.58, 0.42)
24%	9082 (16.0)	1.59 (1.29)	3.17 (2.58)	1.71 (0.97)	596, 616 (0.60, 0.40)
50%	6425 (16.0)	1.19 (0.95)	2.14 (1.71)	1.10 (0.61)	611 (0.61, 0.38)
100%	4346 (16.0)	1.14 (0.86)	1.70 (1.29)	0.99 (0.52)	618 (0.62, 0.37)

[a] Values in the parentheses are the applied driving voltage. [b] Data collected under 20 mA cm^{-2}, while values in the parentheses are the data collected under 100 mA cm^{-2}. [c] Measured at the driving voltage of 8 V.

in Table 3. Obviously, the calculated S_1 and T_1 energy levels for the titled complexes are qualitatively consistent with the 0−0 onset of the absorption (S_1) and phosphorescence (T_1) spectra. Thus, the theoretical level adopted here should be suitable for studying the photophysical properties of these complexes in a qualitative manner. Deviation of the current theoretical approach from the experimental results may plausibly be explained by the negligence of solvation effects in the gas phase ab initio approach.

For the lowest triplet excited state (T_1), the excitations are mainly contributed by HOMO → LUMO and HOMO − 1 → LUMO for both complexes **a** and **b**, in which either HOMO or HOMO − 1 are mainly composed of those indazolate π and Pt(II) d_π orbitals, while LUMO is largely located at the isoquinoline site. As depicted in Figure 6, one can also envisage that the HOMO − 1 orbitals of **3b** and **4b** are apparently much less located at the central Pt(II) atom than HOMO orbitals of **3a** and **4a**, leading to a less MLCT contribution for **3b** and **4b**. For example, results of the calculation show 19.8% (11.6%) MLCT contribution for **3a** (or **4a**), which is significantly larger than the 4.2% (0.2%) for **3b** (or **4b**), consistent with the conclusion drawn on the basis of the experimental results (vide supra). On the other hand, the T_1−S_0 transition of **1b** is mainly composed of HOMO → LUMO (see Table 3), and its MLCT transition character of 16.1% is estimated to be more or less the same as that (17.1%) of **1a**, supporting their similar radiative decay rates deduced experimentally.

The calculated energy gap is also consistent with experimental results, revealing a trend of smaller S_0−S_1 (or S_0−T_1) energy gap for the series **a** complexes. This may be explainable by the difference in orbital contributions on LUMO. Upon carefully viewing Figure 6, it is clear that LUMO of type **a** complexes spreads over the whole 1-iqdz chromophores and pic (or fppz) ligands, while in sharp contrast, the orbital density for the LUMO of **b** complexes is mainly located only on the isoquinoline of 3-iqdz ligands (for **1b**) and pyridyl moieties of pic or fppz ligand (for **3b** and **4b**). Consequently, a lower energy LUMO for type **a** complexes is expected due to its involvement in a stronger π^* delocalization, qualitatively rationalizing their smaller energy gaps compared with type **b** complexes.

Electroluminescent Devices. To demonstrate the capability of exhibiting decent electroluminescent properties, we selected complex **3a** as the representative example as it was synthesized with good yield and hence in a large quantity. The devices incorporating **3a** are then prepared using thermal evaporation, and their structures consist of the multilayer configuration ITO/NPB(40 nm)/CBP:*x* wt % of **3a** (30 nm)/BCP (10 nm)/AlQ_3 (30 nm)/LiF (10 Å)/Al (150 nm), in which NPB, CBP, BCP, and AlQ_3 stand for 1,4-bis(1-naphthylphenylamino)biphenyl, 4,4′-*N*,*N*′-dicarbazolyl-1,1′-biphenyl, 2,9-dimethyl-4,7-diphenyl-1,10-phenanthroline, and tris(8-hydroxyquinolinato) aluminum(III), respectively; while the BCP layer acts as a hole blocker to prevent any emission from AlQ_3. The crucial device performance characteristics are collected in Table 4, showing the systematic trend that varied according to the five dopant concentrations from 6% to 100%. Orange emission was observed for all the concentrations applied, while the one with a pure layer of the

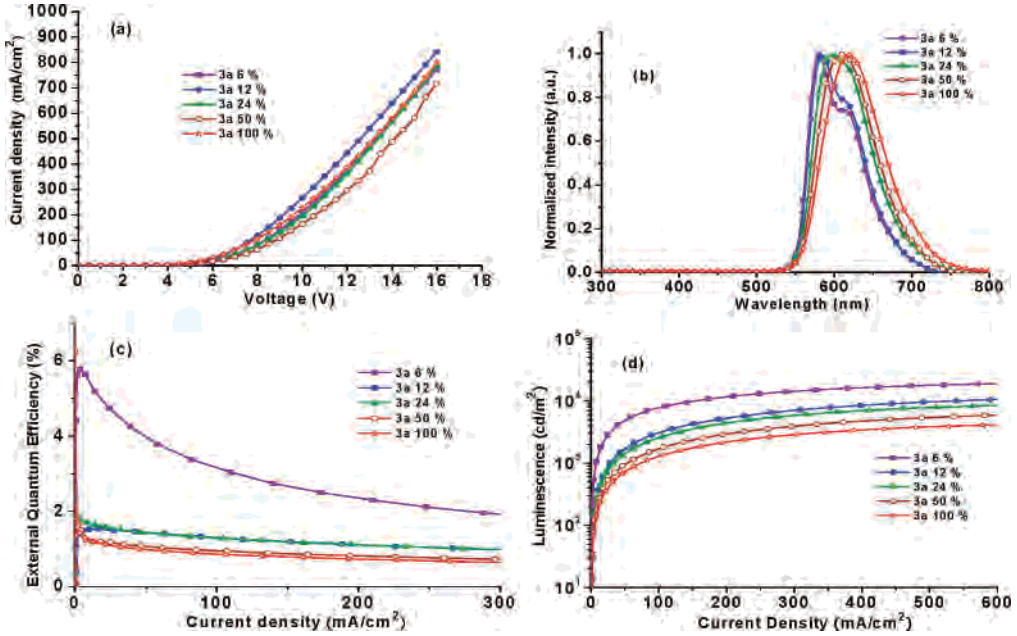

Figure 7. (a) Current density vs applied voltage for the **3a**-doped devices, (b) EL spectra of all devices, (c) external quantum efficiency vs current density, and (d) luminescence vs current density.

Pt(II) emitter showed the lowest brightness and device efficiencies. Figure 7a depicts the current−voltage curves of the electroluminescent devices for **3a** at various doping concentrations, for which the device with 12% **3a** showed the highest current density compared with all other devices operating under identical voltages. Concomitantly, a small red shift of the EL emission was observed with increasing dopant concentrations, e.g., from $\lambda_{max} = 581$ nm for the 6% device to 618 nm for the device with neat dopant (Figure 7b). This red-shifting effect is presumably attributed to the occurrence of a certain degree of intermolecular $\pi\pi$ stacking interaction with increasing concentration of the planar Pt(II) complex. In fact, when comparing the 587 nm emission of **3a** in CH_2Cl_2, a slight red shift of emission was observed for **3a** (621 nm) in the solid state (see Table 2).

Moreover, among varying the dopant concentrations, the best device performance was achieved at 6 wt % (Figure 7c), which rendered a turn-on voltage of 3 V (at 1 cd/m^2) and maximum EQE of 5.78 at 5 V, gave CIE coordinates of (0.57, 0.43) at 8 V, and reached the maximum brightness of 20296 cd/m^2 at a driving voltage of 16 V. Like other phosphorescent OLED devices, their efficiencies also witnessed a significant drop with increasing driving voltage.[22] This can be confirmed by the observation that, at a driving current of 20 mA cm^{-2}, the external quantum efficiency and luminous efficiency are 4.93% and 12.19 cd A^{-1}, while the efficiencies reduced to 3.16% and 7.82 cd A^{-1} at 100 mA cm^{-2}, respectively. For a comparison, recent report on the phosphorescent device fabricated using terdentate cyclometalated Pt(II) complexes showed excellent EL performances in a blended host matrix, for which the data maintained over a four-decade current intensity span and with no significant roll-off.[23]

Finally, as a result of concentration quenching, raising the doping concentration led to a drastic falloff in device efficiencies.[24] Relatively bright luminescence was also observed for other applied concentrations, despite a significant decrease of intensity once the concentration was increased over 6% (Figure 7d), the result of which was evidenced by making a device using 12% of **3a**, showing the reduced maximum EQE of only 1.53 at 5.5 V, maximum brightness of 12248 cd/m^2 at a driving voltage of 16 V, and CIE coordinates of (0.58, 0.42) at 8 V. Upon further increase of the dopant concentration to 100%, the device exhibited a much reduced EQE of 1.14 at 20 mA/cm^2, while the maximum brightness was lowered to only 4346 cd/m^2 at 16.0 V and CIE coordinates was measured to be (0.62, 0.37) at 8 V. We speculate that the lower efficiency at the higher dopant concentration could be due to a combination of two factors, namely the longer emission lifetime of $\tau_{obs} = 8.2$ μs and an increasing degree of aggregation despite its possession of a bulky indazolate fragment. The net results may cause the inferiority of the doped devices mainly associated with triplet−triplet annihilation.

Conclusion

To sum up, we have successfully synthesized two Pt(II) chloride complexes **2a** and **2b** bearing neutral, chelating indazole by treatment of indazole ligands with K_2PtCl_4 in aqueous HCl solution. Although these complexes are non-

(22) (a) Kwong, R. C.; Sibley, S.; Dubovoy, T.; Baldo, M.; Forrest, S. R.; Thompson, M. E. *Chem. Mater.* **1999**, *11*, 3709. (b) Che, C. M.; Hou, Y. J.; Chan, M. C. W.; Guo, J.; Liu, Y.; Wang, Y. *J. Mater. Chem.* **2003**, *13*, 1362. (c) Song, Y. H.; Yeh, S. J.; Chen, C. T.; Chi, Y.; Liu, C. S.; Yu, J. K.; Hu, Y. H.; Chou, P. T.; Peng, S. M.; Lee, G. H. *Adv. Funct. Mater.* **2004**, *14*, 1221.

(23) Cocchi, M.; Virgili, D.; Fattori, V.; Rochester, D. L.; Williams, J. A. G. *Adv. Funct. Mater.* **2007**, *17*, 285.

(24) (a) Adachi, C.; Baldo, M. A.; Forrest, S. R.; Lamansky, S.; Thompson, M. E.; Kwong, P. C. *Appl. Phys. Lett.* **2001**, *78*, 1622. (b) Chen, F. C.; Yang, Y.;Thompson, M. E.; Kido, J. *Appl. Phys. Lett.* **2002**, *80*, 2308.

emissive, the subsequent reaction with additional indazole, sodium picolinate, and even pyridyl pyrazole such as (fppz)H is facile, affording the emissive Pt(II) complexes **1**, **3**, and **4**, respectively. The experimental procedures are efficient and should apply to other synthetic modifications, demonstrating the versatility and the effectiveness of this approach in derivatization of this class of compounds. The respective X-ray structural analysis showed no notable intermolecular Pt···Pt contact, which could be attributed to the steric effect imposed by the bulky indazole fragments. Photoluminescence studies reveal the high quantum yields in the fluid state, short radiative lifetimes in the range of several microseconds. The origin of phosphorescence is attributable to a mixed ^{3}MLCT/$^3\pi\pi$ transition. Consequently, salient differences in photophysical properties such as emission gap and quantum yield between series **a** and **b** complexes are well rationalized by various degrees of π-electron delocalization as well as the MLCT contribution. As for the practical application, complex **3a** was examined for fabrication of phosphorescent OLEDs. Using 6% doping concentration, the maximum EQE of 5.78% at 5 V, and EQE of 4.93%, luminous efficiency of 12.19 cd/A and power efficiency of 6.12 lm W^{-1} at 20 mA/cm^2, and a maximum luminescence of 20296 cd/m^2 at an applied voltage of 16 V were realized. We thus believe that we have added certain contributions to shed light on the fundamental and device properties of the titled Pt(II) complexes. These results should make a promising prospect for future OLEDs based on the strategic design for Pt(II) emitting materials.

Acknowledgment. We thank the following research grants, (NSC 91-2119M-002-016), (NSC 93-2752-M-002-002-PAE), and (94-EC-17A-08-S1-042), for support. We also thank the National Center for High-performance Computing for computer time and facilities.

Supporting Information Available: X-ray crystallographic data file (CIF) of complexes **1b**, **2a**, and **3b**. This material is available free of charge via the Internet at http://pubs.acs.org.

IC700877N